ACS OMEGA

Open Access

http://pubs.acs.org/journal/acsodf

Article

Relativistic DFT Calculations of Cadmium and Selenium Solid-State NMR Spectra of CdSe Nanocrystal Surfaces

Rana Biswas,* Yunhua Chen, Javier Vela, and Aaron J. Rossini

Cite This: *ACS Omega* 2023, 8, 44362−44371

Read Online

ACCESS | Metrics & More | Article Recommendations | Supporting Information

ABSTRACT: Solid-state NMR spectra have been used to probe the structure of CdSe nanocrystals and propose detailed models of their surface structures. Density functional theory (DFT)-optimized cluster models that represent probable molecular structures of carboxylate-coordinated surface sites have been proposed. However, to the best of our knowledge, ^{113}Cd and ^{77}Se chemical shifts have not been calculated for these surface models. We performed relativistic DFT calculations of cadmium and selenium magnetic shielding tensors on model compounds with previously measured solid-state NMR spectra with (i) the four-component Dirac-Kohn−Sham (DKS) Hamiltonian and (ii) the scalar and (iii) spin−orbit levels within the ZORA Hamiltonian. Molecular clusters with Cd and Se sites in varying bonding environments were used to model CdSe (100) and CdSe(111) surfaces capped with carboxylic acid ligands. Our calculations identify the observed ^{113}Cd isotropic chemical shifts δ(iso) of −465, −318, and −146 ppm arising from $CdSeO_3$, $CdSe_2O_2$, and $CdSe_3O$ surface groups, respectively, with very good agreement with experimental measurements. The ^{113}Cd chemical shifts linearly decrease with the number of O-neighbors. The calculated spans ($\delta_{11} - \delta_{33}$) encompass the experimental values for $CdSe_3O$ and $CdSe_2O_2$ clusters but are slightly larger than the measured value for $CdSeO_3$ clusters. Relativistic DFT calculations predicted a one-bond ^{113}Cd−^{77}Se scalar coupling of 258 Hz, which is in good agreement with the experimental values of 250 Hz. With a dense coverage of carboxylic acid ligands, the CdSe (100) surface shows a distribution of Cd−Se bond lengths and *J*-couplings. Relativistic DFT simulations thus aid in interpretation of NMR spectra of CdSe nanocrystals and related nanomaterials.

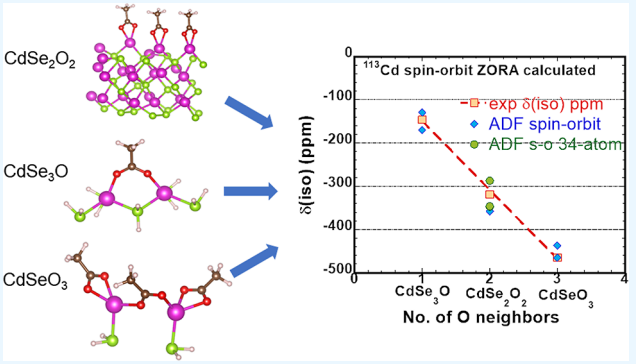

INTRODUCTION

Semiconductor nanocrystal (NC) quantum dots (QDs) have novel tunable electronic and optical properties that depend on their size, shape, and surface passivation.[1−4] Additionally, QD and other NC solar cells exhibit multiple exciton generation (MEG)[5−8] and are hence appealing for photovoltaic applications. NCs are often capped by ligands such as carboxylates, oleates, or phosphonates to prevent NC agglomeration. Furthermore, the extraction of photoexcited carriers from QDs is also critically controlled by their passivating ligands,[9] a feature that is key to the performance of QD solar cells.[10] For NCs that are a few nanometers in diameter, a large fraction of the atoms reside on surface sites. Surface ligands on NCs control their nucleation, growth, colloidal stability, and chemical reactivities.[11−17] Additionally, the surface sites strongly influence the electronic and optical properties of the NC. The importance of surface structure on the optical properties of NCs is well known, and under-coordinated surface atoms with localized electronic states significantly decrease both exciton lifetimes and photo-luminescence quantum yields (PLQYs)[13,18,19] For example, carboxylate-capped CdSe NCs suffer a drop in PLQY when the ligand coverage drops below 3 ligands nm^{-2}.[1,15] A direct correlation between specific surface effects and nonradiative recombination processes has been proposed.[14] It has also been hypothesized that edge and vertex sites on NC surfaces have different ligand binding energies and may be more active in ligand exchange and dissociation reactions.[16] However, direct experimental probes of the molecular structure of NC surfaces are lacking. Hence, it is challenging to directly correlate the molecular level structure of NC surfaces to the photophysical properties.

Solid-state nuclear magnetic resonance (SSNMR) is a powerful tool to determine the structure of NC surfaces and sites on the surface where ligands can bind.[20−22] Additionally, dynamic nuclear polarization (DNP) is a promising method to enhance sensitivity and permit detection of the small fraction of atoms on the surface of NCs.[23−27] Recently, DNP-enhanced

Received: October 3, 2023
Revised: October 11, 2023
Accepted: October 16, 2023
Published: November 6, 2023

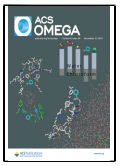

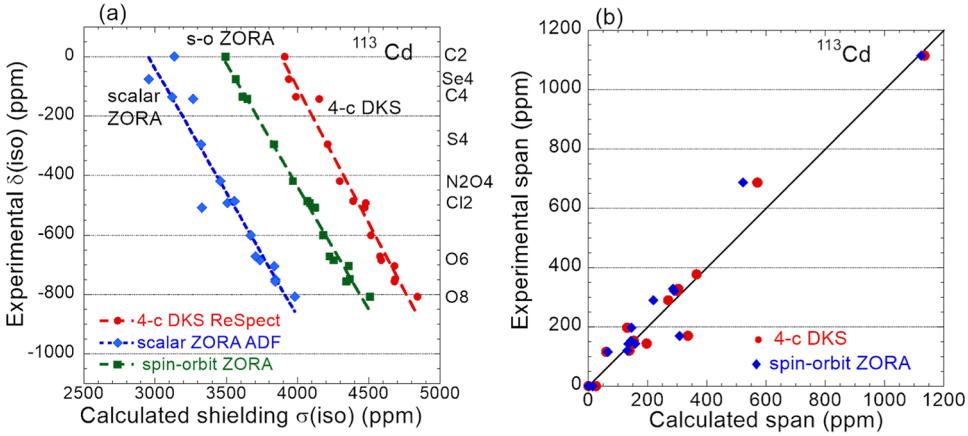

Figure 1. (a) Experimental chemical shifts, δ(iso) for ^{113}Cd in cadmium molecules relative to dimethyl cadmium (Me_2Cd) as the reference, as a function of the calculated isotropic magnetic shieldings, σ(iso), of ^{113}Cd in cadmium molecules. Calculations with 4-c DKS theory (red squares) are compared with scalar ZORA (blue diamonds) and spin−orbit ZORA (green squares). The straight lines represent the best fits. The coordination of the Cd atom is shown on the right for the various compounds. (b) Experimental span ($\Omega = \delta_{11} - \delta_{33}$) for ^{113}Cd in cadmium molecules as a function of the calculated span with 4-c DKS theory and spin−orbit ZORA. The straight line indicates perfect agreement.

^{113}Cd SSNMR spectroscopy was utilized to study the surfaces of zinc blende CdSe NCs with platelet or spheroidal morphologies, which were capped with carboxylic acid ligands.[28] The ^{77}Se and ^{113}Cd cross-polarization magic angle spinning (CPMAS) NMR spectra displayed distinct signals from the surface atoms of the NCs and bulk atoms residing below the surface. 2D ^{113}Cd CP-magic angle turning (MAT) spectra of CdSe nanoplatelets revealed the ^{113}Cd isotropic chemical shifts (δ_{iso}) of −465, −318, and −146 ppm with spans (Ω) of 402, 472, and 364 ppm, respectively. The peak with an isotropic shift of −318 ppm was the most intense. By correlating NMR spectra with the measured infrared (IR) spectra,[29] it was suggested that the δ_{iso} features of −465, −318, and −146 ppm may be assigned to $CdSe_3O$, $CdSe_2O_2$, and $CdSeO_3$ coordination environments for Cd on the surface of the NC. The dominant configuration was suggested to arise from $CdSe_2O_2$ from a chelating termination on the CdSe(100) NC surface.[28] Although these NMR spectral assignments are very reasonable and consistent with measurements, quantum chemical calculations of ^{113}Cd or ^{77}Se magnetic shieldings are lacking. Previous calculations of ^{13}C NMR and infrared spectra of the carboxylate ligands were performed and compared with experimental ^{13}C NMR spectra.[29]

Accordingly, to provide an insight into the Cd and Se bonding environments at NC surfaces, we present relativistic ab initio simulations of the electronic properties and NMR spectra. The ab initio calculations aid interpretations of the observed NMR spectra and the local bonding environments. Furthermore, we compare different levels of relativistic calculations on the calculated ^{113}Cd and ^{77}Se magnetic shieldings and chemical shifts.

RESULTS AND DISCUSSION

Computational Methods and Magnetic Shielding Calibration Curves. Prediction of electronic properties and NMR parameters for lighter elements are routinely performed with density functional theory (DFT) using Gauge Including Projector Augmented Waves (GIPAW)-based solutions of the ZORA Hamiltonian[30] with pseudopotentials and a plane wave basis for electronic wave functions. The well-established pseudopotential plane wave approach implemented in the CASTEP package[31] and other plane wave DFT codes has been very successful for calculating the NMR parameters of lighter elements. However, the plane wave pseudopotential approach is inadequate for heavier elements as relativistic effects are needed to accurately calculate the shieldings of heavy atoms (including Cd and Se). Thus, we have compared results from two relativistic approaches provided by the four-component (4-c) Dirac-Kohn−Sham (DKS) equation in ReSpect[32,33] and the ZORA Hamiltonian with spin−orbit/scalar effects in the Amsterdam Density Functional (ADF)[34−37] packages. The ZORA Hamiltonian with spin−orbit effects has been very successful in simulating the NMR parameters of heavy atoms including Tl−Pt complexes[38,39] and Ce^{IV} complexes.[40]

The solution of the four-component DKS equation with relativistic spin−orbit couplings is provided by the ReSpect electronic structure package with atom-centered Gaussian orbital basis sets and gauge-included atomic orbitals (GIAO) for magnetic shielding calculations. Utilizing the Dirac equation is considered more accurate than incorporating relativistic corrections to the Schrodinger equation.[32] Furthermore, utilizing a fully relativistic formalism provides more accurate NMR parameters not only for heavy atoms but also for the neighboring light atoms that are affected through relativistic spin−orbit effects.[32,41] A special feature in the 4-c DKS theory implemented in ReSpect is the restricted magnetically balanced (RMB) basis sets for the small component of the 4-c wave function.[42,43] The RMB basis avoids strong basis set dependence and yields good agreement with experimental data on shielding of halide molecules.[42] The use of the RMB basis was extended to incorporate the GIAO approach,[43,44] and implemented in the ReSpect package.

The solution of the ZORA Hamiltonian with scalar relativistic and spin−orbit effects in the ADF package is an alternative approach.[34−36] Here, we use both computational approaches to develop calibration relations to correlate the computed relativistic magnetic shieldings of ^{113}Cd and ^{77}Se and compare them with chemical shift tensor parameters from experimental solid-state NMR data.

^{113}Cd Calibration Curves. Holmes and Schurko (HS)[45] performed comprehensive calculations of the ^{113}Cd magnetic shielding tensors of 30 sites in Cd-molecular structures with all electron methods, DFT functionals, and relativistic treatments

https://doi.org/10.1021/acsomega.3c07680
ACS Omega 2023, 8, 44362−44371

and compared them with measured chemical shift tensors to obtain calibration relations. We utilize this comprehensive database of measured chemical shifts to calculate magnetic shieldings using different theoretical methods in this paper. We directly used the geometry-optimized coordinates of Cd-molecules and calculated the magnetic shielding tensors in (i) the four-component DKS formalism (in ReSpect), (ii) the scalar relativistic level with the ZORA Hamiltonian (in ADF), and (iii) with spin−orbit coupling within ZORA Hamiltonian (in ADF), offering a direct comparison between these methods. In order of decreasing isotropic shielding, the molecular structures ranged from Cd coordinated with O8, O6, O5, N2O4, N2O2I2, Cl6, O2N4, S4, Se4, and C2 (Supporting Information: Figures S1 and S2). The measured chemical shifts as a function of the calculated isotropic magnetic shieldings (σ(iso)) are plotted in Figure 1a. Additional information on the molecular structures, charges, shielding tensors, and shielding anisotropy is given in Table S1. The 91-atom $Cd[N(Pri_2PSe)_2]_2$ with Cd tetrahedrally coordinated by 4 Se was the largest molecule calculated (with 1947 large component basis functions in the ReSpect DKS formalism).

We have augmented the HS database, with geometry-optimized dimethyl cadmium and diethyl cadmium, for which the measured chemical shifts in the gas phase and neat forms[46] are tabulated (Table S1). This provides shielding for weakly shielded Cd in a C2 coordination environment (Table S1). Details of the computational methods are given in the Methods section. We use dimethyl cadmium taken as the standard ^{113}Cd chemical shift.[23] The experimentally measured ^{113}Cd chemical shifts for CdSe NCs discussed below were also referenced relative to dimethyl cadmium.

The calculated isotropic shieldings ranged from σ(iso) = (4850, 4500) ppm (ReSpect, ADF SO) for the highly shielded O8-coordinated Cd in cadmium nitrate tetrahydrate ($Cd(NO_3)_2{\cdot}4H_2O$) with a measured chemical shift δ(iso) = −103 ppm; to the least shielded Me_2Cd with σ(iso) = (3908, 3494) ppm; measured δ(iso) = 705 ppm. The ReSpect DKS shieldings are the largest, with the spin−orbit ADF ZORA shieldings ∼360 ppm lower, followed by the ZORA-scalar relativistic shieldings, which are ∼520 ppm lower than the spin−orbit result. This trend is similar to previously calculated ^{119}Sn shieldings in $Sn(Me)_4$,[47] which found scalar ZORA and spin−orbit ZORA shieldings to be 466 and 916 ppm lower, respectively, than the 4c DKS value. For all the three computational methods, the calculated isotropic chemical shifts [δ(iso)] linearly vary with the calculated isotropic shielding [σ(iso)] with the best fit calibration lines given by $\delta(\text{iso}) = C - \alpha\sigma(\text{iso})$ (with C and α in Table 1). ReSpect DKS, spin−orbit ZORA ADF, and scalar ZORA ADF calculations yield slopes of 0.91, 0.836, and 0.829, respectively. Consequently, the spin−orbit and scalar ZORA lines are nearly parallel to each other.

The measured chemical shift tensors δ_{ii}, have been tabulated.[45] Accordingly, we plot the experimental spans ($\delta_{11}-\delta_{33}$) as a function of the calculated span (Figure 1b). The same plot, but for the Haeberlen anisotropy, is shown in Figure S3.

^{77}Se Shielding Calibration Curves. Wasylishen and co-workers[49] have previously performed ZORA DFT calculations of ^{77}Se chemical shifts on a variety of organic and inorganic selenium compounds using ADF. Ashbrook and co-workers[48] recently used planewave GIPAW DFT calculations to predict

Table 1. Calibration Parameters (C, α) in the Relation $\delta(\text{iso}) = C - \alpha\sigma(\text{iso})$ for Predicted Isotropic Chemical Shifts δ(iso) from Calculated Isotropic Shielding σ(iso) for the Different Methods[a]

^{113}Cd (reference Me_2Cd)	C (ppm)	α	mean residual difference (ppm)
ReSpect 4-comp DKS	3526.4	0.908	37
scalar ZORA (ADF)	2470.3	0.836	49
spin−orbit ZORA (ADF)	2876.1	0.829	21
^{77}Se (reference Me_2Se)			
RESPECT 4-comp. DKS	1787.5	0.896	46
spin−orbit ZORA (ADF)	1753.7	0.925	27
scalar ZORA (ADF)	1621.4	0.951	23
DFT-GIPAW (CASTEP)	1453.6	0.891	23
Griffin et al. [ref 48]	1626.0	1.02	
DFT-GIPAW (CASTEP)			

[a]Calculations for ^{113}Cd and ^{77}Se are listed in the upper and lower portions of the table. The DFT ZORA and results from ref 48 are included for ^{77}Se.

^{77}Se chemical shifts for a similar set of compounds. Maaninen et al.[50] utilized plane wave DFT-GIAO calculations to predict ^{77}Se chemical shifts for Se−N compounds. We performed calculations on a set of small Se-containing molecules [$(CH_3)_2Se$, H_2Se, C_4H_4Se, H_2SeO_3, $SeOCl_2$, and $(Ph_2)Se_2$] for which the chemical shifts have been measured.[51] The molecular structures were relaxed with CASTEP plane wave DFT (utilizing GGA exchange−correlation with the PBE functional, ultrasoft pseudopotentials with Koelling−Harmon relativistic treatment, and 450 eV plane wave cutoff). The relativistic shieldings of these geometry-optimized structures were calculated (Figure S4). The experimental chemical shifts are relative to those of the reference compound $(CH_3)_2Se$. The computed shieldings range from 283 ppm for the weakly shielded $SeOCl_2$ to 2289 ppm for strongly shielded H_2Se (Figure 2 and Table S2). The calculated magnetic shieldings

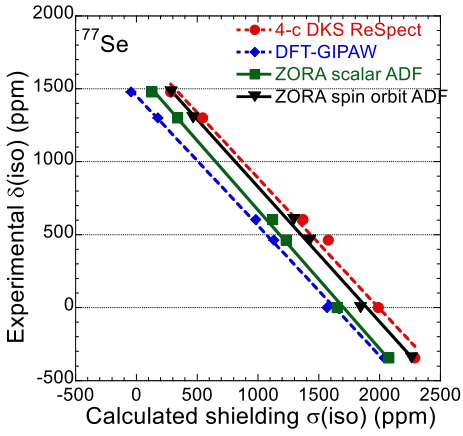

Figure 2. Experimental chemical shifts δ(iso) as a function of the calculated ^{77}Se isotropic magnetic shieldings in small molecules with Se. Our calculations with four-component Dirac-Kohn−Sham (red), ADF-scalar ZORA (green), and spin−orbit ZORA (black) are compared with our DFT-GIPAW calculations. The lines represent the best linear fits to the data. The experimental chemical shifts are relative to the reference compound $(CH_3)_2Se$.

https://doi.org/10.1021/acsomega.3c07680
ACS Omega 2023, 8, 44362−44371

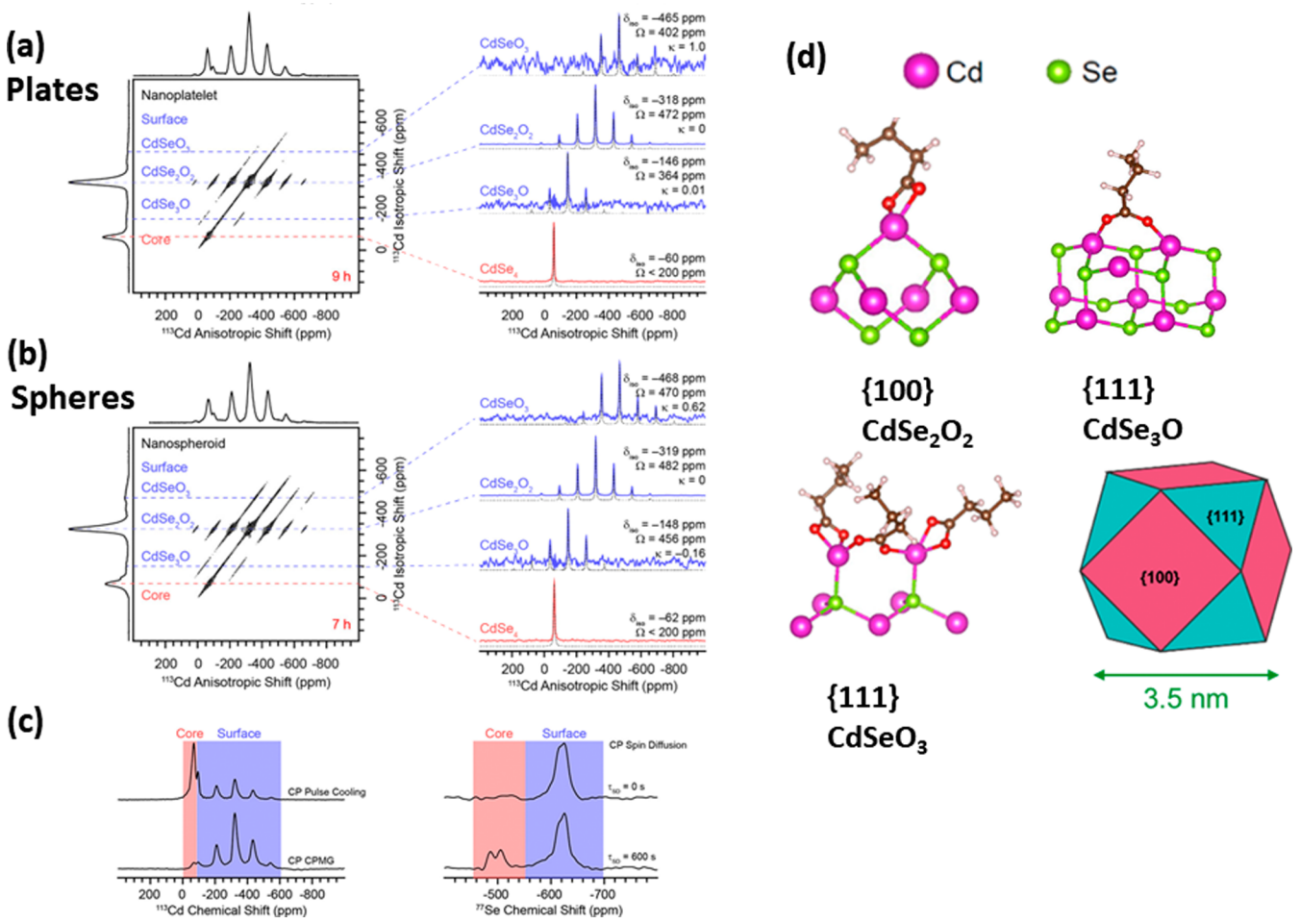

Figure 3. DNP-enhanced surface and core ^{113}Cd and ^{77}Se solid-state NMR spectra of CdSe NCs obtained with an MAS frequency of 10 kHz. (a,b) 2D ^{113}Cd CP-MAT spectra of CdSe nanoplatelets (a) and nanospheroids (b) where the dashed lines indicate distinct ^{113}Cd NMR signals. Individual rows were extracted from the CP-MAT 2D spectrum showing ^{113}Cd sideband manifolds associated with isotropic core and surface NMR signals. (c) ^{113}Cd CP-CPMG and CP pulse cooling spectra of CdSe nanospheroids; ^{77}Se CP-CPMG spin diffusion spectra of CdSe nanospheroids, with spin diffusion times of 0 and 600 s. (d) Representative models of carboxylate-terminated CdSe{100} and {111} facets. Note: Models were obtained without DFT structural optimization. Reprinted (adapted) with permission from Chen et al. *J. Am. Chem. Soc.* **2021**, *143*, 8747−8760. Copyright (2021) American Chemical Society.

vary linearly with the experimentally measured chemical shifts (δ) with the calibration line δ = 1787.5−0.896 σ in four-component DKS (Figure 2). The spin−orbit ZORA level calibration equation is δ = 1753.7−0.925, very close to the 4-c DKS result. The ZORA-scalar and Griffin et al. results[48] are close (Figure 2) to each other. The ZORA-scalar result compares well with previous calibration curves (δ = 1863.4 − 1.01σ') for Se−N compounds.[50] Relativistic methods show agreement between calculated and measured ^{77}Se chemical shifts in organic and inorganic selenium compounds.[49]

We have also calculated shieldings with first-principles DFT calculations utilizing GIPAW for the geometry-optimized molecular structures using CASTEP. The nonrelativistic DFT-GIPAW shieldings (σ') are uniformly ∼360 ppm lower than our calculated values, but the calibration line δ = 1453.5 − 0.891σ' has nearly the same slope. The uniformly shifted calibration line is typical of calculated shielding with and without spin−orbit contributions. The calibration relations are summarized in Table 1.

We calculated the chemical shielding anisotropy (CSA), where CSA = σ_{33} − 0.5(σ_{11} + σ_{22}) with σ_{33} > σ_{22} > σ_{11}. The calculated CSA with relativistic 4-c DKS agrees very well with the DFT-GIPAW calculations (Figure S5) with differences of 20−90 ppm (Table S3), which suggests that the simpler DFT-GIPAW calculations may reasonably estimate chemical anisotropies.

It is of interest to compare the chemical shieldings on the protons that are near-neighbors of Se with the 4-c DKS and DFT-GIPAW. The calculated shieldings with these two approaches agree well (within ∼1 ppm) for most of the molecules considered, where the protons are second neighbors of Se. The notable exception is H_2Se, where the protons are strongly coupled nearest-neighbors of Se, showing a difference of 3 ppm between the two methods (Figure S6). This is consistent with the results from Pb/Sn hydrides, where very large NMR chemical shifts of up to +80 ppm were found for H atoms bonded to Pb or Sn.[52] The extreme ^{1}H chemical shifts in the hydrides arise from the spin−orbit coupling at the heavy atom (HA) mixing triplet states into the ground-state wave function of the molecule, thereby introducing additional shielding at the light atom (LA), referred to as HALA effects.[32]

Modeling ^{113}Cd Solid-State NMR Spectra of NC Surfaces. Recently, DNP-enhanced ^{113}Cd SSNMR spectroscopy was utilized to study surfaces of zinc blende CdSe NCs

https://doi.org/10.1021/acsomega.3c07680
ACS Omega 2023, 8, 44362−44371

with platelet or spheroidal morphologies, which were capped with carboxylic acid ligands.[28] NMR spectra displayed distinct signals from surface atoms of the NCs and bulk atoms residing below the surface. 2D ^{113}Cd CP- magic angle turning (MAT) spectra of CdSe nanoplatelets revealed the ^{113}Cd isotropic chemical shifts δ(iso) of −465, −318, and −146 ppm with spans (Ω) of 402, 472, and 364 ppm, respectively (Figure 3). The peak with $\delta(\text{iso})_{\text{iso}} = -318$ ppm was the most intense.

Here, we create computational models of the local Cd and Se environments present on CdSe NC surfaces passivated by carboxylic acid ligands. Similar structural models were developed by Zhang et al.[29] for CdSe surfaces and the calculation of ^{13}C chemical shifts of carboxylic acid terminated CdSe. We note that Copéret and co-workers previously used $[Cd(SeH_2)_{4-n}(OH_2)_n]^{2+}$ cluster models and ADF ZORA SO calculations to predict the ^{113}Cd chemical shifts as the number of selenium and oxygen atoms were varied in the Cd coordination sphere.[53] They also measured δ(iso) = −310 ppm with Ω = 250 ppm for a carboxylate-capped CdSe NC.[53] Recently, Copéret and co-workers have measured ^{113}Cd chemical shifts on amine-capped CdSe NCs and performed DFT simulations of surface conformations with cluster models.[54] They also obtained δ(iso) = −304 ppm with Ω = 420 ppm for a carboxylate-capped CdSe NC.[54] We have utilized our calibration relations to calculate the relativistic magnetic shielding tensors of ^{113}Cd in CdSe surface models (Table 1).

For the CdSe(100) surface, we generated periodic unit cells passivated with one or three carboxylic acid ligands (Figure 4a,b). To simplify the calculations, acetate ligands were used in place of oleate. We geometry-optimized these structures in CASTEP under the constraint of keeping surface (Cd and Se) in their ideal positions (Figure 4a, charge, q = −1, and Figure 4b, q = −3). We extracted the smallest cluster containing a single acetate group (Figure 4a), capping each outer Se atom with two hydrogen atoms. Geometry optimization of the Se-bound protons resulted in a 14-atom cluster with Cd in $CdSe_2O_2$ coordination with charge q = +1 (Figure 4c). Similarly, the cluster with three acetate groups was extracted from the surface model (Figure 4b), resulting in a 34-atom cluster with hydrogen terminations (SeH_2 or SeH) and $CdSe_2O_2$ coordination for each Cd and charge q = +1 (Figure 4d).

For CdSe(111), we similarly started with a geometry-optimized surface model and generated a cluster with a single acetate group bridging two surface Cd, resulting in a 24-atom cluster with each Cd in $CdSe_3O$ coordination and SeH_2 terminations and q = +3 (Figure 4e). We then constructed a model with each Cd bonded to three O and one Se with q = +1 (Figure 4f). Here, one acetate group bridges neighboring Cd atoms, while another acetate group is bonded to each Cd, resulting in a $CdSeO_3$ coordination geometry (Figure 4f).

The largest cluster utilized was a 56-atom cluster with $CdSe_2O_2$ coordination in which each subsurface Se was bonded to 4 Cd with q = −3 (Figure 4g). S-capping atoms were employed to reduce the computational workload.

We computed the chemical shielding tensors of $CdSe_nO_{4-n}$ sites in each cluster with the three aforementioned relativistic methods (Table 2). Further geometry optimization performed with scalar/SO ZORA (ADF) did not significantly change ^{113}Cd shieldings. From the isotropic shielding σ(iso), we infer the predicted chemical shifts using the calibration relations established for the different methods (Table 1). the

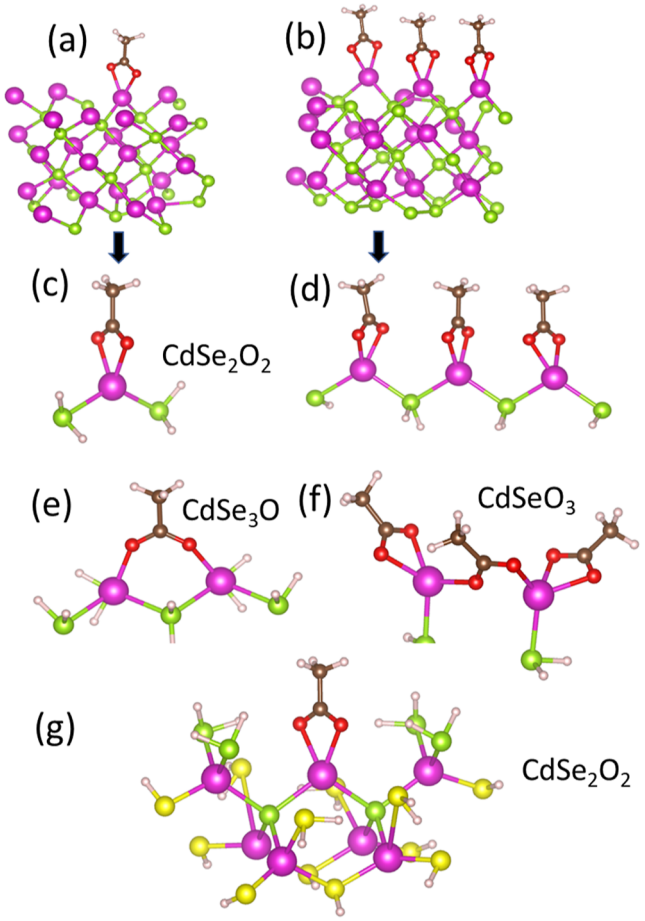

Figure 4. Geometry-optimized configurations of Cd on CdSe(100) and (111) surfaces. (a) CdSe(100) with a single acetate ligand and $CdSe_2O_2$. (b) CdSe(100) with three acetate ligands. (c) 14-Atom $CdSe_2O_2$ cluster. (d) 34-Atom $CdSe_2O_2$ cluster. (e) $CdSe_3O$ cluster with a bridging acetate. (f) $CdSeO_3$ cluster with the bridging acetate group and (g) 56-Atom $CdSe_2O_2$ cluster.

We plot the calculated isotropic chemical shifts δ(iso) for ^{113}Cd for the $CdSe_3O$, $CdSe_2O_2$, and $CdSeO_3$ clusters and compare with the experimental data derived from CdSe nanoclusters (Table 2 and Figure 5). The predicted δ(iso) values encompass the measured δ(iso) for each O-coordination, exhibiting very good agreement between the theory and experiment for all methods. The chemical shifts decrease linearly as the O-coordination around Cd increases (Figure 6) since the Cd is shielded by the electronegative O neighbors. The calculations are at most ∼20−50 ppm lower than the experimental values. This agreement also validates our scheme of building clusters from the periodic structures of CdSe surfaces. It suggests that small (14−34 atom) clusters with SeH_2 and SeH terminations are a reasonable representation of the local structure of CdSe NCs.

The calculated spans ($\Omega = \delta_{11} - \delta_{33}$) bracket the experimental values for $CdSe_3O$ and $CdSe_2O_2$ clusters but are slightly larger (80−160 ppm) than the measured value for $CdSeO_3$ (Figure 6). Calculated values in scalar ZORA (Figure 6b) are higher than the measured spans. The accompanying calculated chemical shielding anisotropy (CSA), $\delta_{33} - 0.5(\delta_{11} + \delta_{22})$, of the Cd molecules and $CdSe_nO_{4-n}$ clusters are shown in Figures S3 and S7. The calculated shieldings of the $CdSe_nO_{4-n}$ clusters with the different theoretical methods are

https://doi.org/10.1021/acsomega.3c07680
ACS Omega 2023, 8, 44362−44371

Table 2. Calculated Isotropic Shieldings σ(iso) and Chemical Shifts δ(iso) for ^{113}Cd for the Different Models with Different Cd Coordination Environments Compared with Measurement[a]

model (from Figure 4)	no. atoms	calc. 4c DKS σ(iso) ppm	calc. 4c DKS δ(iso) ppm	calc. scalar ZORA σ(iso) ppm	calc. scalar ZORA δ(iso) ppm	calc. s-o ZORA σ(iso) ppm	calc. s-o ZORA δ(iso) ppm	exp, δ(iso) ppm
$CdSeO_3$ (f)	29	4477	−479	3583	−462	4108	−465	−465
〃	29	4440	−445	3549	−433	4073	−437	−465
$CdSe_2O_2$ (c)	14	4358	−371	3435	−338	3979	−358	−319
$CdSe_2O_2$ (d)	34	4355	−368	3392	−302	3966	−347	−319
		4286	−306	3350	−267	3893	−287	
		4354	−367	3398	−307	3964	−346	
$CdSe_2O_2$ in CdSe(S) (g)	56	4469	−471	3362	−276	3934	−321	−319
$CdSe_3O$ (e)	24	4092	−130	3145	−95	3703	−129	−146
〃	24	4137	−170	3190	−132	3752	−170	−146
Se (bulk) in $CdSe_2O_2$ CdSe(S) (g)	56	2613	−554	2274	−543			−620
		2601	−543	2280	−549			

[a]Table note: s-o denotes spin−orbit.

shifted by nearly constant values as shown in Figure S8, with the highest shieldings for 4-c DKS, followed by spin−orbit ZORA and scalar ZORA methods. This is similar to the trends found for Cd-molecules in Figure 1a.

^{77}Se NMR Spectra. The 56-atom cluster (Figure 4g) has a surface Cd atom bonded to two Se atoms, which are in turn coordinated with four Cd neighbors. These two Se sites have the same local bonding environment that should be present in surface Se in CdSe(100) NCs and therefore provide a representation of surface Se. With our ^{77}Se calibration relations (Table 1), the calculated ^{77}Se relativistic shieldings for these two sites lead to chemical shifts of −543 and −554 ppm (Table 2) in comparison with measured surface ^{77}Se chemical shifts of −620 ppm.[24] Although the first neighbor shell of Se in the 56-atom cluster (Figure 4g) and the CdSe(100) surface are the same, there are significant differences in the second- and third-neighbor coordination shells between the cluster and the surface. These differences may lead to the difference between the calculated and experimental δ(iso) values.

^{13}C NMR Spectra. The calculated ^{13}C isotropic shieldings σ(iso) (Table S4) with 4-c DKS (ReSpect) show that the C bonded to the acetate group (−COO) is weakly shielded (−13 to −16 ppm), whereas the C in the methyl group is strongly shielded (159−166 ppm). We utilized the ^{13}C calibration relation $\delta(\text{iso}) = -167.3 - 0.9526\cdot\sigma(\text{iso})$ derived earlier for magnetic shielding calculations of small organic molecules correlated with measured chemical shifts.[55] We then obtained calculated chemical shifts of 177−184 ppm [average δ(iso) = 181 ppm] for C in the $CdSe_2O_2$−COO ligand (Table S4) that are in very good agreement with the measured value of 184 ppm.[29] We also obtain δ(iso) = 7−16 ppm [average δ(iso) = 12 ppm] for the C in the methyl group also in very good agreement with the measured value of 10−40 ppm[29] and consistent with known ^{13}C chemical shifts of organic compounds.[56]

***J*-Coupling.** Indirect scalar (*J*-) couplings between ^{113}Cd and ^{77}Se nuclear spins were previously measured with ^{77}Se−^{113}Cd *J*-HMQC and *J*-resolved experiments.[28] These measurements revealed that for core Cd and Se sites, the *J*-coupling was on the order of 75−100 Hz, while for surface selenium and cadmium spin pairs, *J*-couplings of 100 and ca. 250 Hz were observed.

To understand the origin of the observed *J*-couplings, we performed calculations on the simple $CdSe_2O_2$ acetate model (Figure 4c). We calculated the *J*-couplings with a hybrid functional within the ZORA framework and incorporating spin−orbit interactions. This yielded *J*-couplings of 257 Hz (Table S5) between the surface-Cd and the two back-bonded Se (Figure 7a), in excellent agreement with the measured values of 250−255 Hz. For comparison, the 4c DKS formalism for this $CdSe_2O_2$ acetate model yielded J(iso) = 327 Hz, ∼28% larger than the experiment (Table S5). These results suggest that the hybrid functional is a good representation of the indirect *J*-coupling between the nuclear spins. This conclusion is supported by extensive studies of DFT approximations that found hybrid functional families provided the most accurate results.[57]

We also investigated the effect of disorder in the Cd−Se bond lengths in a larger 105-atom CdSe(100) model in which all the eight Cd-surface atoms had carboxyl acid ligands corresponding to a dense coverage of 5.4 ligands/nm^2, as inferred in experimental studies.[28] This larger model yielded several distorted surface Cd configurations with asymmetric Cd−Se and Cd−O bond lengths (Table 3 and Figure S9). The surface undergoes structural distortions that allow the spacing between the ligands to increase, resulting in locally distorted bonding geometries at the surface Cd sites (Table 3). The shorter/longer Cd−Se bond lengths result in a distribution of Cd−Se *J*-couplings, with shorter Cd−Se bonds yielding slightly larger calculated Cd−Se *J*-couplings of 280 and 289 Hz (Figure 7b and Table S5). These calculations suggest that distorted Cd environments on CdSe(100) cannot account for the second Cd−Se *J*-coupling of ca. 100 Hz observed in HMQC experiments.

Since CdSe NCs/nanoplatelets also have (111) facets, we also examined the *J*-couplings of surface Cd−Se in the $CdSeO_3$ bonding configuration expected on CdSe(111) (Figure 4f). Note that we have been unable to measure these *J*-couplings experimentally since the NMR signals from (111) facets are less intense than those from (100) facets. The calculated *J*-couplings $^1J(^{77}\text{Se}_{\text{surf}}-^{113}\text{Cd}_{\text{surf}})$ between surface Cd and its Se neighbor are 111 and 156 Hz (Figure 7c and Table S5). Future NMR experiments should address whether CdSe(111) does indeed have weaker *J*-couplings than CdSe(100). Furthermore, the $^1J(^{77}\text{Se}_{\text{surf}}-^{113}\text{Cd}_{\text{surf}})$ couplings between second-neighbor

https://doi.org/10.1021/acsomega.3c07680
ACS Omega 2023, 8, 44362−44371

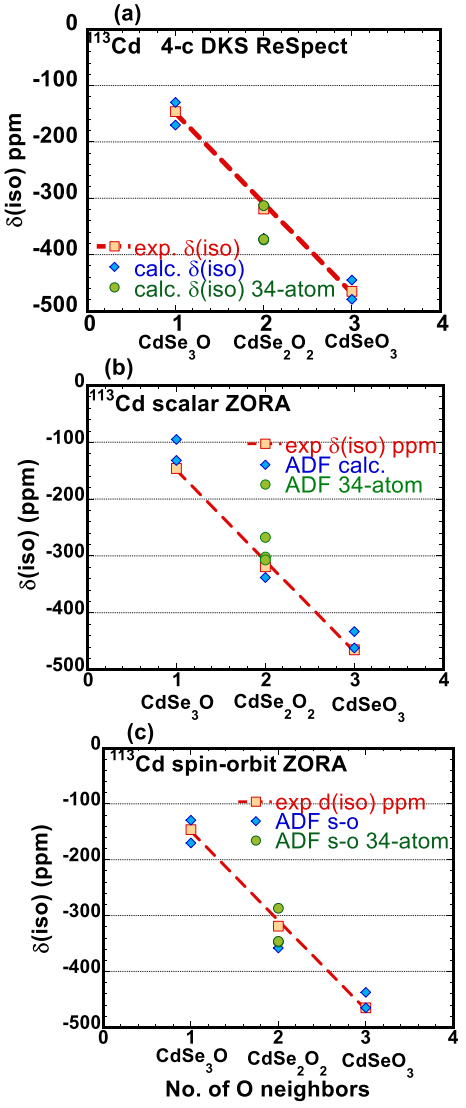

Figure 5. (a) Measured ^{113}Cd isotropic chemical shifts δ(iso) for CdSe nanoclusters passivated with carboxyl acid ligands compared with calculated values from four-component DKS (ReSpect) with increasing O-coordination (N) on Cd. The larger 34-atom $CdSe_2O_2$ cluster is shown as green circles. The line represents the best linear fit to the experimental data δ(iso) = 10.8−159.5*N*. Multiple points for each configuration represent the inequivalent Cd sites. (b) Scalar ZORA (ADF) calculated isotropic chemical shifts compared with measurement using the same conventions. (c) Spin−orbit ZORA (ADF) calculations compared with experimental measurements.

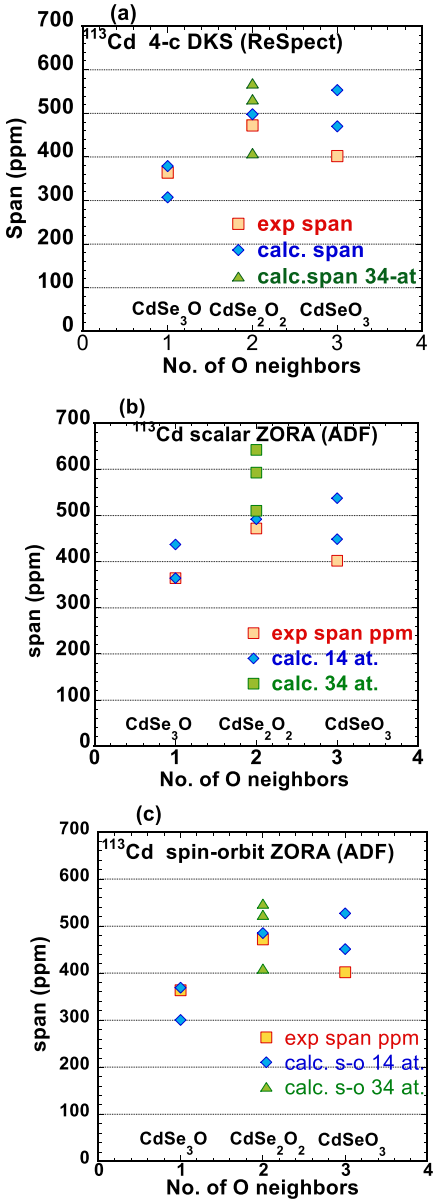

Figure 6. Calculated spans $\Omega = \delta_{11} - \delta_{33}$ for the CdSe clusters with an increasing number of oxygen neighbors. Calculations are with (a) 4-c DKS, (b) scalar ZORA, and (c) spin−orbit ZORA methods.

pairs in the larger 34-atom $CdSe_2O_2$ model (Figure 4d) were negligible (<10 Hz); thus, further neighbor Cd−Se pairs likely do not account for the second *J*(iso) = 85 Hz peak. Also, previously measured $^1J(^{77}Se-^{113}Cd) \sim 120-135$ Hz[S8] for the $Cd[N(Pri_2PSe)_2]_2$ molecule with tetrahedral Cd−Se_4 coordination is more similar to the measured $^1J(^{77}Se_{core}-^{113}Cd_{core})$ = 105 Hz from core Cd−Se sites.

We used calculations to also predict the two-bond ^1J couplings between surface Cd and C in $CdSe_2O_2$ on CdSe(100) (in the acetate group; Figure 4a). These calculations gave an average ^{113}Cd−^{13}C *J*-couplings of 69 and 76 Hz, using the hybrid ZORA and 4-c DKS calculations, respectively (Table S5). Again, these couplings have not been experimentally measured, but the calculations suggest that they should be measurable and should be the target of future studies. The predicted results for the wurtzite CdSe(010) surfaces are summarized in the Supporting Information (Figure S10 and Table S6).

CONCLUSIONS

We have performed all-electron relativistic DFT calculations of cadmium and selenium magnetic shielding tensors with (i) the four-component Dirac-Kohn−Sham (DKS) Hamiltonian, (ii) the scalar level ZORA Hamiltonian, and (iii) spin−orbit level within the ZORA Hamiltonian. Calculations for Cd-containing molecular clusters with varying bonding environments and coordinations (C2, C4, Se4, S4, N2O4, N4O2, N2O2I2, O6Cl2, O6, and O8) were used to generate a calibration relation between magnetic shielding tensors and chemical shifts for ^{113}Cd. We similarly simulated magnetic shielding tensors in Se-containing molecules with different bonding

https://doi.org/10.1021/acsomega.3c07680
ACS Omega 2023, 8, 44362−44371

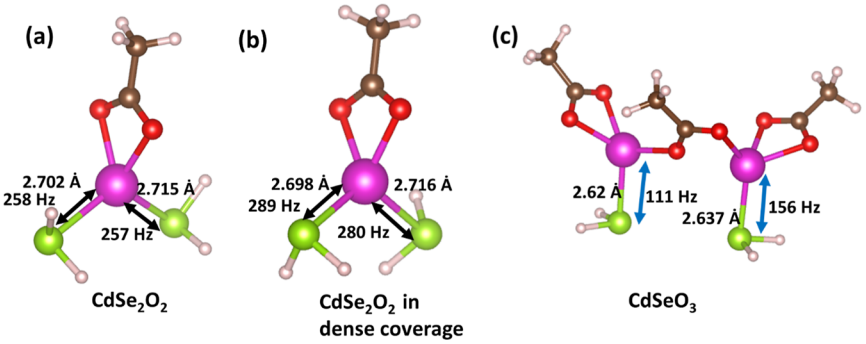

Figure 7. (a) $CdSe_2O_2$ model showing the *J*-couplings between surface ^{113}Cd and bonded ^{77}Se (arrows). (b) Geometry-optimized structure of a $CdSe_2O_2$ model obtained from a CdSe(100) surface densely covered with acetate ligands with bond-lengths and J-couplings. (c) Geometry of $CdSeO_3$ on the CdSe(111) surface, showing bond lengths and *J*-couplings.

Table 3. Bond Lengths at the Cd Sites of the CdSe(100) Surface Are Densely Packed with Acetate Ligands

Cd site	CdSe bond lengths (Å)	Cd O bond lengths (Å)
Cd 1	2.643, 2.657	2.244, 2.358
Cd 5	2.577, 2.947	2.32, 2.30
Cd 8	2.559, 2.633	2.387, 2.48
Cd 9	2.60, 2.839	2.213, 2.405
Cd 12	2.587, 2.758	2.254, 2.336
Cd 13	2.629, 2.660	2.30, 2.304

environments (C2, H2, O3, Se, and C), which generated calibration relations between magnetic shielding tensors and chemical shifts for ^{77}Se. The four-component DKS Hamiltonian offered the highest shielding, followed by spin−orbit ZORA and scalar ZORA methods. The linear calibration for each method had similar slopes and was linearly shifted relative to each other for ^{113}Cd and ^{77}Se.

Geometry-optimized cluster models were made to represent CdSe(100) and CdSe(111) surfaces capped with carboxylic acid ligands. We utilized our relativistic DFT calibration to identify the SSNMR observed ^{113}Cd isotropic chemical shifts δ(iso) of −465, −318, and −146 ppm to $CdSeO_3$, $CdSe_2O_2$, and $CdSe_3O$ surface groups. Relativistic DFT shows a linear decrease of ^{113}Cd chemical shifts δ(iso) with the number of O-neighbors, as Cd becomes more shielded, with very good agreement between calculation and measurement. The calculated spans bracket the experimental values for $CdSe_3O$ and $CdSe_2O_2$ clusters but are slightly larger (80−160 ppm) than the measured value for $CdSeO_3$ clusters. From the calculated surface ^{77}Se shieldings in a larger 56-atom cluster in which the surface Se have a similar bonding environment as in a CdSe(100) NC, we calculated δ(iso) for ^{77}Se of −542 to −557 ppm, which compare with the measured value of −620 ppm for surface ^{77}Se in CdSe NCs. Calculations also reproduced the one-bond ^{113}Cd−^{77}Se *J*-couplings. The hybrid functional within the ZORA is most accurate for the ^{1}J couplings, although the shieldings within the hybrid formalism and the nonhybrid spin−orbit levels of theory are very similar. Taken together, the ability of relativistic DFT calculations to construct cluster models of surface species and accurately predict NMR parameters for heavy nuclei can be a powerful tool to probe the surface structure in a variety of inorganic semiconductor NCs.

METHODS

The ReSpect all-electron calculations were performed with (i) the standard dyall-vdz 21s14p10d2f basis set with 127 Gaussian-type orbitals (GTOs) for Cd; (ii) [14s11p6d] basis for Se (77 GTOs); (iii) dyall-vdz 10s6p1d basis set for C (33 GTO's), and (iv) upc-1 4s1P orbitals for H (7 GTO's). The $Cd[N(Pri_2PSe)_2]_2$ 91-atom molecule had 1947 Cartesian GTOs—nearly the largest feasible structure in ReSpect. The nonrelativistic simulations were used as an input to the full four-component Dirac equation in ReSpect. The relativistic Dirac Kohn−Sham (DKS) formalism utilized the PBE0 density functional.[15] Self-consistent field calculations converged within 30 steps for energies and chemical shielding tensors.

The ADF simulations utilized the TZ2P-J all-electron basis for all elements, generalized gradient approximation (GGA) and PBE density functionals for exchange and correlation. The scalar ADF and spin−orbit coupling calculations were performed with a ZORA Hamiltonian. CdSe fragments were geometry-optimized. The hybrid functional used a PBE0 functional with 25% Hartree−Fock exchange and was more computationally intensive. All relativistic DFT simulations were performed on parallel computing clusters using 8−64 cores. The spin−spin *J*-coupling was the sum of the diamagnetic, paramagnetic, Fermi contact (FC) and spin diffusion (SD) contributions, with the FC + SD contributions being the dominant one.

ASSOCIATED CONTENT

Supporting Information

The Supporting Information is available free of charge at https://pubs.acs.org/doi/10.1021/acsomega.3c07680.

Details of molecular structures (PDF)

AUTHOR INFORMATION

Corresponding Author

Rana Biswas − *U.S. Department of Energy Ames National Laboratory, Ames, Iowa 50011, United States; Department of Physics and Astronomy; Electrical & Computer Engineering; Microelectronics Research Center, Iowa State University, Ames, Iowa 50011, United States;* orcid.org/0000-0002-0866-2100; Email: biswasr@iastate.edu

Authors

Yunhua Chen − *U.S. Department of Energy Ames National Laboratory, Ames, Iowa 50011, United States; Department*

https://doi.org/10.1021/acsomega.3c07680
ACS Omega 2023, 8, 44362−44371

of Chemistry, Iowa State University, Ames, Iowa 50011, United States

Javier Vela − *U.S. Department of Energy Ames National Laboratory, Ames, Iowa 50011, United States; Department of Chemistry, Iowa State University, Ames, Iowa 50011, United States;* orcid.org/0000-0001-5124-6893

Aaron J. Rossini − *U.S. Department of Energy Ames National Laboratory, Ames, Iowa 50011, United States; Department of Chemistry, Iowa State University, Ames, Iowa 50011, United States;* orcid.org/0000-0002-1679-9203

Complete contact information is available at: https://pubs.acs.org/10.1021/acsomega.3c07680

Notes

The authors declare no competing financial interest.

■ ACKNOWLEDGMENTS

This work was supported by the U.S. Department of Energy (DOE), Office of Science, Basic Energy Sciences, Materials Science and Engineering Division. The research was performed at Ames National Laboratory, which is operated for the U.S. DOE by Iowa State University under contract DE-AC02-07CH11358. We acknowledge the use of computational resources at the National Energy Research Scientific Supercomputing Center (NERSC) which is supported by the Office of Science of the U.S. DOE under contract no. DE-AC02-05CH11231. We thank Dr. Frederic Perras for access to the ADF computational package and Dr. G. Laurent and Dr. M. Hanrahan for valuable discussions.

■ ABBREVIATIONS

DNP, dynamic nuclear polarization; SSNMR, solid-state nuclear magnetic resonance; DFT, density functional theory; DKS, Dirac-Kohn−Sham; 4c, four component; ZORA, zero-order regular approximation; ReSpect, relativistic spectroscopy DFT program package; ADF, Amsterdam Density functional package; GGA, generalized gradient approximation; TZ2P, triple-ζ with two polarization functions; HMQC, hetero-molecular quantum correlation; PBE, Perdew−Burke−Ernzerhof; GGA, generalized gradient approximation; CP, cross-polarization; CPMG, Carr−Purcell−Meiboom−Gill

■ REFERENCES

(1) Boles, M. A.; Ling, D.; Hyeon, T.; Talapin, D. V. The Surface Science of Nanocrystals. *Nat. Mater.* **2016**, *15*, 141−153.

(2) Smith, A. M.; Nie, S. Semiconductor Nanocrystals: Structure, Properties, and Band Gap Engineering. *Acc. Chem. Res.* **2010**, *43* (2), 190−200.

(3) Efros, A. L., Lockwood, D. L., Tsybeskov, L., Eds. In *Semiconductor Nanocrystals from Basic Principles to Applications, Nanostructure Science and Technology*; Springer Science+Business Media: New York, 2003.

(4) Rogach, A. L.; Klar, T. L.; Lupton, J. M.; Meijerink, A. D.; Feldmann, J. Energy transfer with semiconductor nanocrystals. *J. Mater. Chem.* **2009**, *19*, 1208−1221.

(5) Nozik, A. J. Quantum dot solar cells. *Phys. E* **2002**, *14* (1−2), 115−120.

(6) Beard, M. Multiple Exciton Generation in Semiconductor Quantum Dots. *J. Phys. Chem. Lett.* **2011**, *2*, 1282−1288.

(7) Beard, M.; Midgett, A. G.; Law, M.; Semonin, O. E.; Ellingson, R. J.; Nozik, A. J. Variations in the quantum efficiency of multiple exciton generation for a series of chemically treated PbSe nanocrystal films. *Nano Lett.* **2009**, *9*, 836−845.

(8) Kamat, P. V. Quantum Dot Solar Cells. The Next Big Thing in Photovoltaics. *J. Phys. Chem. Lett.* **2013**, *4* (6), 908−918.

(9) Xu, J.; Voznyy, O.; Liu, M.; Kirmani, A. R.; Walters, G.; Munir, R.; Abdelsamie, M.; Proppe, A. H.; Sarkar, A.; García de Arquer, F. P.; et al. 2D matrix engineering for homogeneous quantum dot coupling in photovoltaic solids. *Nat. Nanotechnol.* **2018**, *13* (6), 456−462.

(10) Choi, M. J.; García de Arquer, F. P.; Proppe, A. H.; Seifitokaldani, A.; Choi, J.; Kim, J.; Baek, S. W.; Liu, M.; Sun, B.; Biondi, M.; et al. Cascade surface modification of colloidal quantum dot inks enables efficient bulk homojunction photovoltaics. *Nat. Commun.* **2020**, *11*, 103.

(11) Talapin, D. V.; Lee, J.-S.; Kovalenko, M. V.; Shevchenko, E. V. Prospects of Colloidal Nanocrystals for Electronic and Optoelectronic Applications. *Chem. Rev.* **2010**, *110*, 389−458.

(12) Hartley, C. L.; Kessler, M. L.; Dempsey, J. L. Molecular-Level Insight into Semiconductor Nanocrystal Surfaces. *J. Am. Chem. Soc.* **2021**, *143*, 1251−1266.

(13) Owen, J. The Coordination Chemistry of Nanocrystal Surfaces. *Science* **2015**, *347*, 615−616.

(14) Saniepay, M.; Mi, C.; Liu, Z.; Abel, E. P.; Beaulac, R. Insights into the Structural Complexity of Colloidal CdSe Nanocrystal Surfaces: Correlating the Efficiency of Nonradiative Excited-State Processes to Specific Defects. *J. Am. Chem. Soc.* **2018**, *140*, 1725−1736.

(15) Ernzerhof, M.; Scuseria, G. Assessment of the Perdew-Burke-Ernzerhof exchange-correlation functional. *J. Chem. Phys.* **1999**, *110*, 5029−5036.

(16) Drijvers, E.; De Roo, J.; Martins, J. C.; Infante, I.; Hens, Z. Ligand Displacement Exposes Binding Site Heterogeneity on CdSe Nanocrystal Surfaces. *Chem. Mater.* **2018**, *30*, 1178−1186.

(17) Chen, D.; Lei, H.; Zhu, C.; Chen, X.; Tian, H.; Fang, W.; Qin, H.; Peng, X. Epitaxial Integration of Multiple CdSe Quantum Dots in a Colloidal CdS Nanoplatelet. *J. Am. Chem. Soc.* **2022**, *144*, 8444−8448.

(18) Nagpal, P.; Klimov, V. Role of mid-gap states in charge transport and photoconductivity in semiconductor nanocrystal films. *Nat. Commun.* **2011**, *2* (1), 486.

(19) Voznyy, O.; Thon, S. M.; Ip, A. H.; Sargent, E. H. Dynamic Trap Formation and Elimination in Colloidal Quantum Dots. *J. Phys. Chem. Lett.* **2013**, *4*, 987−992.

(20) Axelson, D. E. *Solid State Nuclear Magnetic Resonance: A Practical Introduction*; CreateSpace Independent Publishing Platform, 2012.

(21) Bryce, D. L.; Gee, M.; Wasylishen, R. E. High-Field Chlorine NMR Spectroscopy of Solid Organic Hydrochloride Salts: A Sensitive Probe of Hydrogen Bonding Environment. *J. Phys. Chem. A* **2001**, *105* (45), 10413−10421.

(22) Ryan, B. J.; Hanrahan, M. P.; Wang, Y.; Ramesh, U.; Nyamekye, C. K. A.; Nelson, R. D.; Liu, Z.; Huang, C.; Whitehead, B.; Wang, J.; et al. Silicene, Siloxene, or Silicane? Revealing the Structure and Optical Properties of Silicon Nanosheets Derived from Calcium Disilicide. *Chem. Mater.* **2020**, *32*, 795−804.

(23) Apperley, D. C.; Harris, R. K.; Hodgkinson, P. *Solid State NMR Basic Principles and Practice*; Momentum Press: NY, 2012.

(24) Rossini, A. J.; Zagdoun, A.; Hegner, F.; Schwarzwälder, M.; Gajan, D.; Copéret, C.; Lesage, A.; Emsley, L. Dynamic Nuclear Polarization NMR Spectroscopy of Microcrystalline Solids. *J. Am. Chem. Soc.* **2012**, *134* (40), 16899−16908.

(25) Maly, T.; Debelouchina, G. T.; Bajaj, V. S.; Hu, K.-N.; Joo, C.-G.; Mak-Jurkauskas, M. L.; Sirigiri, J. R.; Van Der Wel, P. C. A.; Herzfeld, J.; Temkin, R. J.; Griffin, R. G. Dynamic nuclear polarization at high magnetic fields. *J. Chem. Phys.* **2008**, *128* (5), 052211.

(26) Ni, Q. Z.; Daviso, E.; Can, T. V.; Markhasin, E.; Jawla, S. K.; Swager, T. M.; Temkin, R. J.; Herzfeld, J.; Griffin, R. G. High frequency dynamic nuclear polarization. *Acc. Chem. Res.* **2013**, *46* (9), 1933−1941.

(27) Corzilius, B. High-field dynamic nuclear polarization. *Annu. Rev. Phys. Chem.* **2020**, *71*, 143−170.

(28) Chen, Y.; Dorn, R. W.; Hanrahan, M. P.; Wei, L.; Blome-Fernandez, R.; Medina-Gonzalez, A.; Adamson, M. A. S.; Flintgruber, A. H.; Vela, J.; Rossini, A. J. Revealing the Surface Structure of CdSe Nanocrystals by Dynamic Nuclear Polarization-Enhanced ^{77}Se and ^{113}Cd Solid-State NMR Spectroscopy. *J. Am. Chem. Soc.* **2021**, *143*, 8747−8760.
(29) Zhang, J.; Zhang, H.; Cao, W.; Pang, Z.; Li, J.; Shu, Y.; Zhu, C.; Kong, X.; Wang, L.; Peng, X. Identification of Facet-Dependent Coordination Structures of Carboxylate Ligands on CdSe Nanocrystals. *J. Am. Chem. Soc.* **2019**, *141* (39), 15675−15683.
(30) Pickard, C. J.; Mauri, F. All-electron magnetic response with pseudopotentials: NMR chemical shifts. *Phys. Rev. B: Condens. Matter Mater. Phys.* **2001**, *63*, 245101.
(31) Clark, S. J.; Segall, M. D.; Pickard, C. J.; Hasnip, P. J.; Probert, M. I. J.; Refson, K.; Payne, M. C. First principles methods using CASTEP. *Z. Kristallogr.* **2005**, *220* (5−6), 567−570.
(32) Repisky, M.; Komorovsky, S.; Kadek, M.; Konecny, L.; Ekström, U.; Malkin, E.; Kaupp, M.; Ruud, K.; Malkina, O. L.; Malkin, V. G. ReSpect: Relativistic spectroscopy DFT program package. *J. Chem. Phys.* **2020**, *152*, 184101.
(33) Komorovsky, S.; Jakubowska, K.; Świder, P.; Repisky, M.; Jaszuński, M. NMR Spin−Spin Coupling Constants Derived from Relativistic Four-Component DFT Theory—Analysis and Visualization. *Phys. Chem. A* **2020**, *124* (25), 5157−5169.
(34) te Velde, G.; Bickelhaupt, F. M.; Baerends, E. J.; Fonseca Guerra, C.; van Gisbergen, S. J. A.; Snijders, J. G.; Ziegler, T. Chemistry with ADF. *J. Comput. Chem.* **2001**, *22*, 931−967.
(35) Wolff, S. K.; Ziegler, T.; van Lenthe, E.; Baerends, E. J. Density functional calculations of nuclear magnetic shieldings using the zeroth-order regular approximation (ZORA) for relativistic effects: ZORA nuclear magnetic resonance. *J. Chem. Phys.* **1999**, *110*, 7689−7698.
(36) Autschbach, J. The role of the exchange-correlation response kernel and scaling corrections in relativistic density functional nuclear magnetic shielding calculations with the zeroth-order regular approximation. *Mol. Phys.* **2013**, *111*, 2544−2554.
(37) Autschbach, J. Relativistic calculations of magnetic resonance parameters: Background and some recent developments. *J. Philos. Trans. A* **2014**, *372*, 20120489.
(38) Ducati, L. C.; Marchenko, A.; Autschbach, J. NMR J-coupling constants of Tl-Pt bonded metal complexes in aqueous solution: Ab-initio molecular dynamics and localized orbital analysis. *Inorg. Chem.* **2016**, *55*, 12011−12023.
(39) Chen, W.; Liu, F.; Matsumoto, K.; Autschbach, J.; Le Guennic, B.; Ziegler, T.; Maliarik, M.; Glaser, J. Spectral and structural characterization of amidate-bridged platinum-thallium complexes with strong metal-metal bonds. *Inorg. Chem.* **2006**, *45*, 4526−4536.
(40) Panetti, G. B.; Sergentu, D.-C.; Gau, M. R.; Carroll, P. J.; Autschbach, J.; Walsh, P. J.; Schelter, E. J. Isolation and characterization of a covalent CeIV-Aryl complex with an anomalous ^{13}C chemical shift. *Nat. Commun.* **2021**, *12*, 1713.
(41) Malkin, V. G.; Malkina, O. L.; Salahub, D. R. Spin-orbit correction to NMR shielding constants from density functional theory. *Chem. Phys. Lett.* **1996**, *261*, 335−345.
(42) Komorovský, S.; Repiský, M.; Malkina, O. L.; Malkin, V. G.; Malkin Ondík, I.; Kaupp, M. A fully relativistic method for calculation of nuclear magnetic shielding tensors with a restricted magnetically balanced basis in the framework of the matrix Dirac−Kohn−Sham equation. *J. Chem. Phys.* **2008**, *128*, 104101.
(43) Komorovský, S.; Repiský, M.; Malkina, O. L.; Malkin, V. G. Fully relativistic calculations of NMR shielding tensors using restricted magnetically balanced basis and gauge including atomic orbitals. *J. Chem. Phys.* **2010**, *132*, 154101.
(44) Repiský, M.; Komorovský, S.; Malkina, O. L.; Malkin, V. G. Restricted magnetically balanced basis applied for relativistic calculations of indirect nuclear spin−spin coupling tensors in the matrix Dirac−Kohn−Sham framework. *Chem. Phys.* **2009**, *356*, 236−242.
(45) Holmes, S. T.; Schurko, R. W. A DFT/ZORA Study of Cadmium Magnetic Shielding Tensors: Analysis of Relativistic Effects and Electronic-State Approximations. *J. Chem. Theory Comput.* **2019**, *15*, 1785−1797.
(46) Kidambi, S. A.; Ramamoorthy, A. Quantum Chemical calculations of Cadmium Chemical shifts in inorganic complexes. *J. Phys. Chem. A* **2002**, *106*, 10363−10369.
(47) Malkin, E.; Komorovsky, S.; Repisky, M.; Demissie, T. B.; Ruud, K. The Absolute Shielding Constants of Heavy Nuclei: Resolving the Enigma of the ^{119}Sn Absolute Shielding. *J. Phys. Chem. Lett.* **2013**, *4*, 459−463.
(48) Griffin, J. M.; Knight, F. R.; Hua, G.; Ferrara, J. S.; Hogan, S. W. L.; Woollins, J. D.; Ashbrook, S. E. ^{77}Se Solid-State NMR of Inorganic and Organoselenium Systems: A Combined Experimental and Computational Study. *J. Phys. Chem. C* **2011**, *115*, 10859−10872.
(49) Demko, B. A.; Eichele, K.; Wasylishen, R. E. A Combined Experimental and Quantum Chemistry Study of Selenium Chemical Shift Tensors. *J. Phys. Chem. A* **2006**, *110*, 13537−13550.
(50) Maaninen, T.; Tuononen, H.; Kosunen, K.; Oilunkaniemi, R.; Hiitola, J.; Laitinen, R.; Chivers, T. Formation, Structural Characterization, and Calculated NMR Chemical Shifts of Selenium-Nitrogen Compounds from $SeCl_4$ and ArNHLi (Ar = supermesityl, mesityl). *Z. Anorg. Allg. Chem.* **2004**, *630* (12), 1947−1954.
(51) Duddeck, H. *Landolt-Börnstein: Numerical Data and Functional Relationships in Science and Technology - New Series*, 35G 2004 ed.; Landolt-Bornstein New Series III/35G Selenium-77 NMR; Lechner, M. D., Gupta, R. R., Eds.; Springer; May 25, 2004.
(52) Vícha, J.; Marek, R.; Straka, M. High-Frequency ^{1}H NMR Chemical Shifts of Sn^{II} and Pb^{II} Hydrides Induced by Relativistic Effects: Quest for Pb^{II} Hydrides. *Inorg. Chem.* **2016**, *55*, 10302−10309.
(53) Piveteau, L.; Dirin, D. N.; Gordon, C. P.; Walder, B. J.; Ong, T. C.; Emsley, L.; Copéret, C.; Kovalenko, M. V. Colloidal-ALD-Grown Core/Shell CdSe/CdS Nanoplatelets as Seen by DNP Enhanced PASS−PIETA NMR Spectroscopy. *Nano Lett.* **2020**, *20*, 3003−3018.
(54) Cao, W.; Yakimov, A.; Qian, X.; Li, J.; Peng, X.; Kong, X.; Coperet, C. Surface Sites and Ligation of Amine-capped CdSe Nanocrystals. ChemRxiv: 10.26434/chemrxiv-2022-d0s34, **2022**.
(55) Hanrahan, M. P.; Venkatesh, A.; Carnahan, S.; Calahan, J. L.; Lubach, J.; Munson, E. J.; Rossini, A. J. Enhancing the Resolution of ^{1}H and ^{13}C Solid-State NMR Spectra by Reduction of Anisotropic Bulk Magnetic Susceptibility Broadening. *Phys. Chem. Chem. Phys.* **2017**, *19*, 28153−28162.
(56) Gunther, H. *NMR Spectroscopy-An Introduction*; John Wiley, 1998, Chapter X.
(57) Goerigk, L.; Hansen, A.; Bauer, C.; Ehrlich, S.; Najibi, A.; Grimme, S. A look at the density functional theory zoo with the advanced GMTKN55 database for general main group thermochemistry, kinetics and noncovalent interactions. *Phys. Chem. Chem. Phys.* **2017**, *19*, 32184−32215.
(58) Demko, B. A.; Wasylishen, R. E. A Solid-State NMR investigation of single-source precursors for group 12 metal selenides; $M[N(^iPr_2PSe)_2]_2$ (M = Zn, Cd, Hg). *Dalton Trans.* **2008**, No. 4, 481−490.

https://doi.org/10.1021/acsomega.3c07680
ACS Omega 2023, 8, 44362−44371